Chemical Engineering Journal 144 (2008) 79–87

Contents lists available at ScienceDirect

Chemical Engineering Journal

journal homepage: www.elsevier.com/locate/cej

Overall chemical kinetics model for partial oxidation of methane in inert porous media

K.V. Dobrego [a,*], N.N. Gnesdilov [a], S.H. Lee [b], H.K. Choi [b]

[a] Luikov Heat and Mass Transfer Institute, Belarus Academy of Sciences, 15 P. Brovka Street, Minsk 220072, Belarus
[b] Korean Institute of Energy research (KIER), 71-2 Jang-dong, Yuseong-gu, Daejeon 305-343, Republic of Korea

ARTICLE INFO

Article history:
Received 16 January 2008
Received in revised form 24 April 2008
Accepted 13 May 2008

Keywords:
Methane partial oxidation
Syngas
Filtration combustion
Simulation
Chemical kinetics model

ABSTRACT

An overall three-step six-component chemical kinetics model which includes $CH_4 + O_2 \rightarrow CO + H_2O + H_2$ and reversible $2CO + O_2 \longleftrightarrow 2CO_2$ and $CH_4 + H_2O \longleftrightarrow CO + 3H_2$ reactions is elaborated for the simulation of partial oxidation of methane in inert porous media. Procedure of the model adjusting to the experimental data is described. Kinetic parameters of the model are derived on the basis of temperature–flow rate, H_2 and CO output concentration–flow rate and temperature–pressure experimental correlations. It is found that extremely slow solid body temperature growth with flow rate $T_{s,max}(G)$ reported in the works on partial oxidation of methane (and other hydrocarbons) in inert porous media may be reproduced by the model. The model is designed for optimization, scale up and design assistance of the reactors of partial oxidation of methane.

It is demonstrated that the overall chemical kinetics model can be combined with detailed gas-phase kinetics model for the investigation of detailed composition of syngas and intermediary components.

1. Introduction

Energy demands of the modern society stimulate the exploration of new energy technologies. High expectations are linked to the natural gas (predicted to outlast the oil reserves [1]) conversion to chemical feedstock, transportation fuels and hydrogen. Analysis shows [2] that conversion to synthesis gas (syngas) and its further utilization is more effective for industrial application than direct methane conversion to heavy hydrocarbons. There are three main processes of methane to syngas conversion: carbon dioxide reforming, water steam reforming and partial oxidation (POX). The last is exothermic, which provides certain technological advantages [3,4].

Considerable efforts were made for the improvement of catalytic POX technologies [2–7] and consequent synthesis of methanol, dimethylether and other chemicals [4] during the past decades. Commercial catalytic generators of syngas/reduction atmospheres are produced by AirLiquide, BP and some other companies. The industrial scale non-catalytic POX process was first implemented on the petrochemical plant in Bintulu, Malaysia, by Shell [3,8] (oxygen and steam entrained flow, $T \sim 1400\,^{\circ}C$, $P = 5–7$ MPa). Presently a number of industrial plants convert natural gas to syngas in oxygen-steam atmosphere by the entrained flow technology [9].

Usage of air instead of oxygen may decrease the POX price dramatically, although in this case the syngas is diluted with nitrogen (55–60%), and adiabatic temperature of the POX process (see Table 1) remains too low for intensive reaction and favorable conversion degree. One of the promising technologies suitable for the methane–air POX is, so-called superadiabatic (excess enthalpy) filtration combustion (FC) in inert porous media (PM).

The main principles of filtration combustion (excess enthalpy combustion) were formulated in the works by Weinberg [10], Fateev [11], Matros [12] and were further developed in [13–18] and other works. The corner stone of the superadiabatic FC is interaction (or coupling) of propagating thermal and combustion waves resulting in local increase of enthalpy and superadiabatic temperature.

FC applications concentrate mostly on the extra lean and the extra rich mixtures combustion. The latter gained considerable attention in the past decades in connection with syngas and hydrogen production. Important work in this area was performed in Heat and Mass Transfer Institute, Minsk [22–25], University of Illinois, Chicago [26–28], University of Texas, Austin [29], University of Erlangen-Newrenberg [30] and some other centers.

Other technologies that utilize excess enthalpy effects in two-phase systems were investigated in works by Weinberg et al. [19], Itaya et al. [20], Pedersen-Mjaanes [21] and others. Weinberg et al. [19] experimented with rich methane–air mixtures (equivalence ratio $\Phi \sim 2$) in spouted bed reactor. They reported up to 19.5% H_2 and 12.6% CO content in flue gas and methane conversion rate up to 95% (calculated by remaining CH_4) for the maximum temperature

* Corresponding author. Tel.: +375 284 20 21; fax: +375 284 22 12.
E-mail address: kdob@itmo.by (K.V. Dobrego).

1385-8947/$ – see front matter © 2008 Elsevier B.V. All rights reserved.
doi:10.1016/j.cej.2008.05.027

Table 1
Equilibrium temperature and H_2 concentration for methane–air POX for the given pressure p and equivalence ratio Φ

	p = 1 atm		p = 2 atm		p = 4 atm		p = 8 atm	
	T_{ad} (K)	Y_{H_2}	T_{ad} (K)	Y_{H_2}	T_{ad} (K)	Y_{H_2}	T_{ad} (K)	Y_{H_2}
Φ = 1	2225	3.60e−03	2240	3.05e−03	2253	2.57e−03	2264	2.15e−03
Φ = 2	1565	0.1762	1565	0.1762	1565	0.1762	1565	0.1762
Φ = 3	1030	0.3212	1049	0.3149	1074	0.3059	1106	0.2946
Φ = 4	929	0.3196	962	0.308	997	0.2953	1033	0.2813
Φ = 5	900	0.2986	931	0.2868	965	0.2738	999	0.2595

Adiabatic conditions, T_0 = 300 K. Thermodynamic calculation.

in the bed ∼1100 °C. In the works [20,21] hydrogen production in methane–air flame stabilized within the porous media was investigated. Gas mixture was fed though the porous ceramic plate and ignited at the exit [20]. The upper flammability limit was estimated as Φ = 2.5 in equivalence ratio (defined as molar fuel to air ratio related to its stoichiometric value $\Phi = (F/A)/(F/A)_0$ for methane–air combustion. Hydrogen concentration in flue gas was up to 10% in mole fraction, which is close to the thermodynamic equilibrium at characteristic for the surface burner temperatures.

Higher superadiabatic conditions for POX can be obtained in transient co-flow FC wave. In the typical investigation [29] a co-flow FC wave in sponge-type ceramics was considered. The temperature of the porous media as well as the concentration of the main components was measured for the range of equivalence ratios Φ = 1.5–5. The measured conversion ratio of methane was up to 70%. The numerical simulation, utilizing detailed gas-phase kinetics, overestimated the temperature by 300–500 K, reproducing main trends and dependences of the process quite adequately.

In the works [22–25] POX process was examined in different packed beds (Al_2O_3, SiO_2, ZrO_2). The temperature and the concentration of the main components were measured as a function of mixture flow rate and equivalence ratio. It was found that conversion ratio directly correlates with the maximum temperature of the packed bed. The temperature growth slowed down dramatically at higher flow rates so that the maximum temperature T_{max} did not exceed 1450 °C in all the experiments for Φ = 4. This fact has not found an adequate explanation [23]. The better conversion ratio was reached at some lower $\Phi \sim 3$ [24], while absolute concentration of hydrogen at the exit of the system did not change considerably with equivalence ratio variation from 2.5 to 4. It is interesting to note that no deposited soot was found inside porous media at filtration combustion in inert alumina and zirconia at equivalence ratios as high as $\Phi \sim 4$ [23,24].

At the end of 80th investigation of regenerative type FC reactors (also called Reverse Flow or Reciprocal Flow Reactor (RFR)) was started [17,31]. Superadiabatic conditions are realized in RFR in the transient co-flow wave, while periodic switching of the flow direction results in establishing of periodic quasi-steady regime of operation. Currently RFR technology may be considered as the most worthwhile option for practical applications.

The development of the FC POX process, its scale up and optimization demand profound numerical, particularly non-steady and in some cases 2D simulation. The choice of appropriate chemical kinetics model, enough compact for fast calculations and adequate to the process, is the stumbling block here. The detailed kinetic mechanisms developed for gas-phase oxidative processes like GRI 3.0, Konnov's, Warnatz's [32–34] and similar can hardly be applied to this task because of their bulkiness (50 and more components are included). Moreover, investigations show that utilization of the detailed kinetics does not ensure an adequate reproduction of the FC systems parameters, particularly the maximum temperature of the porous media [25,29]. On the other hand, the integration of the kinetic equations along the temperature profiles established experimentally gives good agreement with measured gas components output concentrations [31]. This is because of the fact that gas composition is strongly determined by thermodynamic equilibrium (although it can be far from equilibrium), while the low-temperature "ignition" kinetics is not adequate to the filtration combustion. Although the standard two-temperature volume-averaged model of filtration combustion does not account for the shape of the PM particles and detailed hydrodynamics [25,35], an inadequate model of POX kinetics is the main source of mistakes.

In [25] the method of correction of Konnov's model (applicable to other models too) was proposed. The idea was to add the scheme with the plausible reaction of radical production $O_2 \rightarrow O + O$ and to adjust its rate by using experimental data. This method lets one tune precisely the ignition temperature but does not simplify detailed model or improves its adequacy in other aspects.

Considerable efforts were paid to develop kinetic mechanisms of the methane partial oxidation on catalysts [2,36,37]. Microkinetic models for partial oxidation and reforming of methane on Pt [36] and Rh [37] were proposed and validated. Note that rather complicated models consisting of more than 100 heterogeneous reactions and bulky gas-phase reactions subset were incapable of predicting H_2 and CO selectivity and were tuned in its methane oxidation subset [37]. The necessity of handling such a bulky mechanism is of the question in view of limited number of the measured parameters. Anyway, the utilization of catalytic POX models for modeling the POX in inert porous media is groundless.

Considering the above-mentioned point, one can conclude that formulation of the compact chemical kinetics model providing the quantitative adequacy of modeling is an important task for extensive numerical study of the partial oxidation of methane.

An overall three-step six-component chemical kinetics model for the simulation of partial oxidation of methane is described in this article. The method/algorithm of its adjusting to experimental data is proposed, which makes the model rather universal. The correlations between maximum temperature, H_2, CO output concentrations and specific mass flow rate—$T_{s,max}(G)$, $X_{H_2}^{exit}(G)$, $X_{CO}^{exit}(G)$ are used as the basic experimental data. The kinetic constants and parameters of the model are obtained. The model can be applied to filtration combustion POX reactors numerical simulation, optimization, scaling up and design assistance.

2. Methane partial oxidation in inert porous media experimental data

There is a lack of published experimental data on partial oxidation of methane in inert porous media. The most important "primary" information about the POX in transient FC conditions is obtained in single wave experiments. Available information includes one-dimensional temperature profiles of the porous media, porous media maximum temperature $T_{s,max}$, main components output concentration as a function of gas mass flow rate

Table 2
Parameters of the system for the standard case POX reactor, experiments [23,24]

Parameter	Dimension	Value	Description
L	m	0.38	Reactor (porous media) length
D_0	m	0.038	Internal diameter of the reactor chamber
d_0	m	6×10^{-3}	Packed bed particle diameter
L_{isl}	m	0.06	Thermal insulation layer width
β	W/(m^3 K)	389	Volumetric heat loss coefficient
p_0	Pa	1.013×10^5	Pressure at exit of reactor
ε	–	0.6	Emissivity of the PM particle surface
m	–	0.4	Porosity
ρ_s	kg/m^3	2810	PM particle material density
c_s	J/(kg K)	794	PM particle material thermal capacity
λ_s	W/(m K)	0.2	Thermal conduction coefficient of the porous media
λ_{isl}	W/(m K)	0.1	Thermal conduction coefficient of insulation material
D_p, D_τ	m^{-1}	0.5, 0.1	Dispersion coefficients
Φ	–	4	Fuel–oxidizer equivalence ratio
α	W/(m^3 K)	$\sim 10^5$	Gas–solid heat transfer coefficient
G_m	kg/(m^2 s)	Variable	Gas mixture mass specific flow rate

Packed bed—Al_2O_3 balls.

(or filtration velocity), mixture equivalence ratio and gas composition.

A typical laboratory scale reactor [22,23] consists of a quartz tube (D = 41 mm, L = 500 mm) isolated outside with 5 cm KAOWOOL blanket, packed with ceramic particles—Al_2O_3 cylinders or balls (from 3 to 6 mm diameters), ZrO_2 grains or SiO_2 chips (other data are in Table 2). The system is ignited by the stoichiometric mixture combustion near the beginning of the reactor. The measurements are performed after FC wave is formed and quasi-steady regime is established. Thermocouples are usually used for the temperature measurements with a characteristic accuracy of ~1%. Other uncertainties are associated with the radial position of thermocouples. Fig. 1 presents some selected data of PM maximum temperature $T_{s,max}$ measurement (marks) [23,24,29]. Comparison of these temperatures with the correspondent adiabatic temperatures (Table 1) gives the understanding of the "superadiabatic" effect, which takes place at FC.

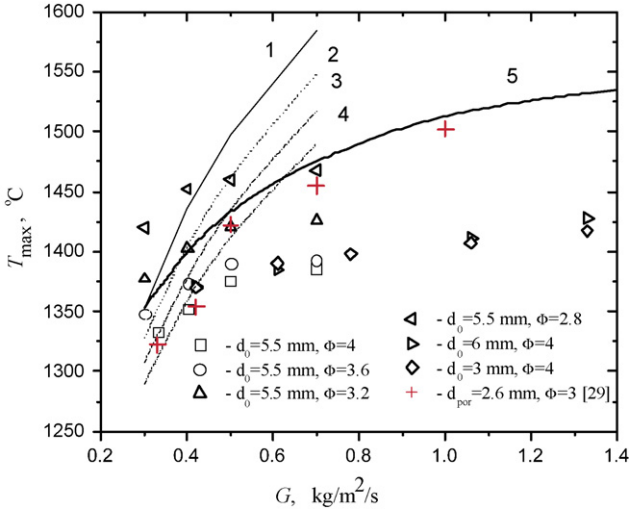

Fig. 1. Porous media maximum temperature T_{max} as a function of mass specific flow rate G_m. Experimental [23,24,29] (marks) and calculated (lines) data. 1–4: calculated by using startup overall kinetic model for Φ = 2.8, 3.2, 3.6 and 4 correspondingly; 5: by using GRI 3.0 kinetics, Φ = 4. d_0 = 5.5 mm.

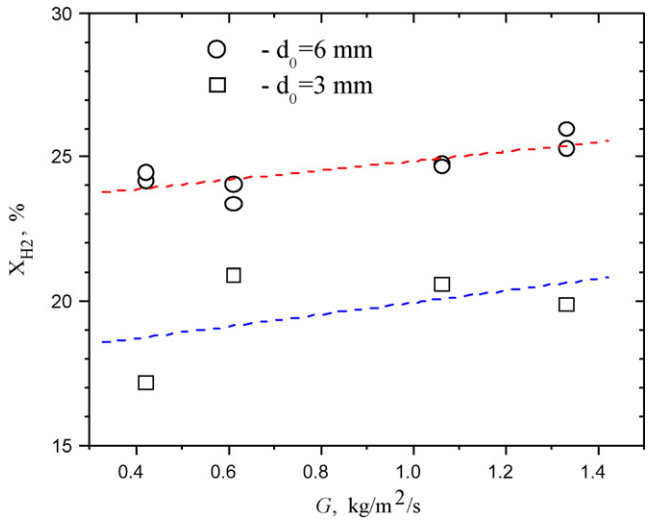

Fig. 2. H_2 concentration $X_{H_2}^{exit}$ as a function of mass specific flow rate. Measured points [23] (marks) and their approximants (dashed lines). Packing of Al_2O_3 balls d_0 = 3 and 6 mm. Φ = 4.

The main components concentrations (molar fractions) X_{H_2}, X_{CO}, X_{CH_4} and X_{N_2} are measured in the most experimental works. Figs. 2 and 3 show selected data on H_2 concentration in dried flue gas and H_2 to CO concentration ratio [23]. The packed beds made of alumina balls with diameter 3 and 6 mm were considered. In spite of rather high dispersion of the experimental data, the observed tendencies (dashed lines) and averaged (expected) values of concentrations can be utilized for the numerical model verification and adjusting.

The concentration of the main components at the exit of reactor as a function of the mixture equivalence ratio $\Phi \sim 1$–3 and oxygen content in oxidizer for the fixed specific mass flow rate $G \cong 0.13$ kg/(m^2 s) is presented in [27,28].

Experiments reported in [29] were performed in quartz tube rector (D_0 = 45 mm, L = 356 mm) placed in ceramic thermal insulation shell and filled with yttria-stabilized zirconia sponge-

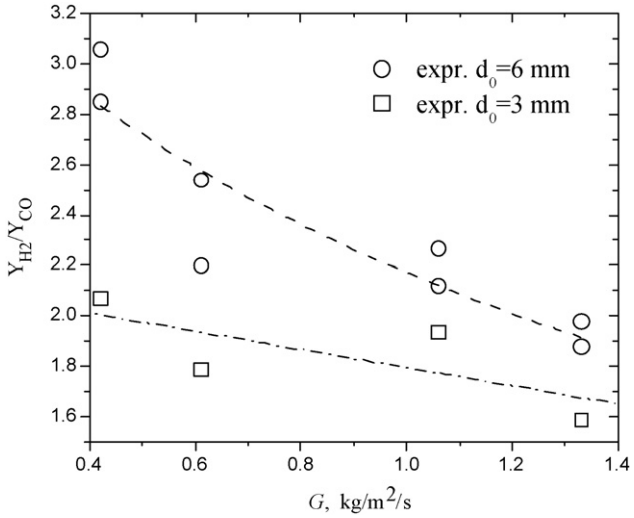

Fig. 3. H_2 and CO concentrations ratio at the exit of reactor $X_{H_2}^{exit}/X_{CO}^{exit}$ as a function of mass specific flow rate. Experimental data [23] (marks), and their approximants (dashed lines). Packing of Al_2O_3 balls d_0 = 3 and 6 mm. Φ = 4.

type ceramics (porosity $m = 0.835$, characteristic pores diameter $d_{por} = 2.6$ mm). Porous media maximum temperature and main components concentrations at the exit were measured for $\Phi = 1.5$–5 at constant Darcy velocity (superficial flow velocity) $u_D = 0.55$ m/s, as well as for different filtration flow rates at fixed equivalence ratio $\Phi = 3$. The last data from [29] are represented in Fig. 1 with crosses and demonstrate similarity to the data obtained for alumina-packed bed porous media at moderate flow rates $G = 0.4$–0.6 kg/(m^2 s). In the wider range of flow rates the stronger temperature growth is observed, which is presumably connected with the small pressure drop in foamed PM.

Experimental data of POX reactor operation at elevated pressure could be of great value in connection with industrial application of the process. Unfortunately, there is no consistent published data on FC POX at elevated pressures. To emulate pressure-dependent characteristics ($T_{s,max} = f(p), X_{H_2}^{exit} = f(p)$ and similar) numerical simulation with detailed chemical kinetics model can be considered.

3. Model of the filtration combustion methane partial oxidation reactor

Experimental reactor described in [23,24] was a prototype for numerical modeling. The accepted parameters of the reactor system are listed in Table 2.

3.1. Basic equations

For the simulation of the system a conventional volume-averaged two-temperature approximation was used [15,25,29,35]. The model assumes porous body a homogeneous media with effective (volume averaged) properties. The set of equations included continuity and filtration equations for gas, mass conservation equation for chemical components, thermal conductivity equations for gas and solid phase and ideal gas state equation. An unsteady problem was considered to simulate system evolution in accordance with experimental tests:

$$\frac{\partial \rho_g}{\partial t} + \nabla(\rho_g \mathbf{u}) = 0, \tag{1}$$

$$-\nabla p = \frac{\mu}{k_0}\mathbf{u} + \frac{\rho_g}{k_1}|\mathbf{u}|\mathbf{u}, \tag{2}$$

$$\rho_g \frac{\partial Y_i}{\partial t} + \rho_g \mathbf{u}\nabla Y_i - \nabla \rho_g \mathbf{D}\nabla Y_i = \dot{\rho}_i, \tag{3}$$

$$\rho_g c_p \frac{\partial T_g}{\partial t} + c_p \rho_g \mathbf{u}\nabla T_g - \nabla \Lambda \nabla T_g = \frac{\alpha_{vol}}{m}(T_s - T_g) - \sum_i h_i \dot{\rho}_i, \tag{4}$$

$$(1-m)\rho_s c_s \frac{\partial T_s}{\partial t} - \nabla(\lambda \nabla T_s) = \alpha_{vol}(T_g - T_s) - \beta(T_s - T_0), \tag{5}$$

$$\rho_g = \frac{pM}{RT_g}. \tag{6}$$

Here m is the porosity, Y_i is the mass fraction of ith component, β is the heat loss coefficient, T_0 is the ambient temperature, h_i is the mass enthalpy of the ith component, $\dot{\rho}_i$ is the ith component mass generation rate due to chemical reactions (it is described in the chemical model section), subscripts "g" and "s" relate to gas and solid phases, respectively and other parameters are standard. Note that the model is formulated for mass fractions Y_i, while the analysis and comparison with experimental data are performed for molar fractions X_i.

The gas diffusivity and conductivity terms in Eqs. (3) and (4) is a sum of the gas molecular transport and dispersion terms: $D = D_g + D_D$ and $\Lambda = \lambda_g + \Lambda_D$. The dispersion terms are expressed via the bed particle diameter d_0 [38]: $D_D = 0.1 d_0 u_g$ and $\Lambda_D \equiv 0.1 d_0 u_g (c\rho)_g$. The thermal conductivity of the porous medium includes the solid matrix conductivity λ_s and radiation diffusivity terms:

$$\lambda = \lambda_{s,e} + \left(\frac{16}{3}\right)\varepsilon\sigma T^3 d_{ph}, \tag{7}$$

where $\sigma = 5.67 \times 10^{-8}$ W/(m^2 K^4) is the Stefan-Boltzmann constant, ε is the emissivity of the porous medium surface, $d_{ph} = (2m/(3(1-m)))d_0$ is the average photon free path; the solid matrix effective conductivity is a very weak (compared to radiation diffusion) function of temperature and can be expressed by the empirical formula [47] $\lambda_{s,e} = \lambda_g(\lambda_s/\lambda_g)^{0.28-0.757\log m - 0.057\log(\lambda_s/\lambda_g)}$, λ_s is the thermal conductivity of solid matter.

The volumetric convective heat transfer coefficient α_{vol} is used in the form suggested by [38]:

$$\alpha_{vol} = \left(\frac{6m}{d_0^2}\right)\lambda_g Nu, \quad Nu = 2 + 1.1 Pr^{1.3} Re^{0.6}. \tag{8}$$

The molar heat capacity and enthalpy of each substance as well as the average enthalpy per mole of the mixture H are calculated by the polynomial formulas in accordance with the CHEMKIN procedures and database [39]. Other temperature-dependent gas properties (μ, D_g, λ_g) were calculated by explicit approximate formulas, with a characteristic accuracy of 5% in the entire temperature range [18,40]. (Note that in the FC system dispersion prevails over molecular transport, and this makes the problem of accurate calculation of D_g, λ_g insignificant.)

3.2. Boundary conditions

The system (1)–(5) is supplemented with boundary conditions for temperature, concentration and filtration velocity. As far as the 1D system was simulated, the boundary conditions were applied to the input ($x = 0$) and output ($x = L$) cross-sections of the reactor. Condition of heat exchange with circumambience was applied to Eq. (5):

$$\lambda \frac{\partial T_s}{\partial x}\bigg|_{x=0,x=L} = \varepsilon\sigma(T_s^4 - T_0^4) + \alpha_{ext}(T_s - T_0). \tag{9}$$

Conditions of zero diffusion flows through the chamber boundaries $\partial Y_i/\partial x$ ($x = 0$, L) $= 0$ were applied to Eq. (3). To avoid uncontrollable diffusion flows through the inlet and outlet sections, the appropriate diffusion coefficients were set equal to zero $D(x = 0) = D(x = L) = 0$. The composition of the input gas was specified: $Y_i(x = 0) = Y_i^{entrance}$.

Similar conditions were applied to Eq. (4): $\partial T_g/\partial x(x = 0, L) = 0$. The temperature of the input gas was fixed: $T_g(x = 0) = T_0$.

Boundary condition for gas filtration consists of condition of wall impermeability, given mass flow rate at the inlet cross-section and constant pressure at the outlet cross-section $p(x = L) = p_0$.

The side losses of the system in the 1D case were simulated by applying the proper value to the heat loss coefficient β in energy equation (5). This procedure is proved to be adequate for the thermally isolated FC systems [40,41]. The heat loss coefficient β can be easily estimated under the assumption that predominant part of the total temperature drop in the system ($T_{max} - T_0$) comes to insulation layer and heat flux is in the steady state (time averaged value of β):

$$\beta = \frac{2\lambda_{isl}}{R_0^2 \ln(R_2/R_0)}, \tag{10}$$

where R_0 is the internal radius of the reactor chamber and R_2 is the external radius of the system including the thermal insulation

layer. The heat loss coefficients evaluated by (10) for the standard reactor is presented together with other parameters in Table 2.

The initial temperature of gas and solid has a step-type profile with the maximum temperature 1500 K and length of the step 5 cm. Reactor contains air at the initial instant.

3.3. Chemical kinetics overall model

Nowadays it seems impossible to consistently *ab initio* generate an adequately detailed chemical kinetics mechanism for filtration combustion POX modeling. The reasonable alternative is to utilize simplified thermodynamically agreed overall reaction model adjusted to experimental data.

The model suitable for the POX reactors scale up and optimization in the certain range of parameters $\{G, p, \Phi, \ldots\}$ should guarantee the following:

1. correspondence of calculated correlation $T_{s,max} = f(G)$ to experimental data;
2. correspondence of calculated correlation $T_{s,max} = f(p)$ to experimental data;
3. correspondence of calculated $X_{H_2}^{exit}$ and X_{CO}^{exit} ($X_{H_2}^{exit}/X_{CO}^{exit}$) to experimental data.

Lets us consider the simple three-step six-component kinetic model including one irreversible and two reversible stages:

$$CH_4 + O_2 \xrightarrow{k_1} CO + H_2O + H_2, \quad (11)$$

$$2CO + O_2 \overset{k_2, k_{-2}}{\rightleftarrows} 2CO_2, \quad (12)$$

$$CH_4 + H_2O \overset{k_3, k_{-3}}{\rightleftarrows} CO + 3H_2. \quad (13)$$

Our choice is determined, in the first place, by the fact that the scheme generally corresponds to main overall fluxes of the components transformation in the system. (Note that the reaction (11) corresponds to a concept that methane oxidation goes through a combination of partial and complete oxidation reactions see for example [37], although details of the reaction routes are still unclear.) Second, reactions are not strongly coupled (cross-dependent), which let one effectively adjust the parameters of the system. The first reaction dominates at the beginning of the process when oxygen is an abundant component, the last one (water reforming) prevails after main oxygen is consumed and actually determines methane conversion degree. The influence of the second reaction is limited due to a very small equilibrium concentration of oxygen in the system, nevertheless it allows one to control the concentration ratio $X_{H_2}^{exit}/X_{CO}^{exit}$.

Mass generation of the kth component due to jth reaction is calculated according to the kinetic equation:

$$\dot{\rho}_k \equiv \rho \frac{dY_k}{dt} = -s_{kj} z_j \exp\left(\frac{E_j}{T}\right) M_k \left(\frac{\rho}{M_i}\right)^{\sum_i p_i} \prod_i Y_i^{p_i}, \quad (14)$$

where s_{kj} is the stoichiometric coefficients for the kth component, jth equation; z_j is the pre-exponent factor of the rate constant; E_j is the activation energy (here in K units); p_i is the applied orders of reaction by ith chemical component (default $p_{ij} = s_{kj}$); M_i is the molar mass of the ith component. The above-expanded form of the kinetic equation is used in the 2DBurner software package [42] and let one apply arbitrary orders to each component and to the total order of the reaction by pressure by assigning a specified value to the sum $\sum_i p_i = \text{ORDER}$.

The three-step six-component model is the minimum system capable of approximating experimental dependencies named above in the section. Assuming that the reverse reactions rates are evaluated by equilibrium constants, we have seven parameters to be fitted according to experimental data: $z_1, E_1, z_2, E_2, z_3, E_3$, ORDER—the total order by pressure for reactions (11)–(13). These parameters are constant in all range of p, G.

The procedure of the kinetic model parameters adjusting consists of the following. The experimental FC POX reactor is simulated by using the model (1)–(10) and arbitrary parameters of the kinetic model (11)–(13). Here the parameters of one-stage, second-order methane oxidation reaction, used for FC simulation [46] $k = 2.17 \times 10^8 \exp(15{,}640/T)$ were applied to reactions (11)–(13) at the beginning. Based on the experimental data and dependency $T_{s,max} = f(G)$, the kinetic parameters for reaction (11) are fitted. Afterwards the constants of the reaction (13) are adjusted based on experimental data for $X_{H_2}^{exit}$ and correlation $X_{H_2}^{exit}(G)$. Taking as a basis the experimental data for $X_{CO}^{exit}(G)$ and characteristic trend of $X_{H_2}^{exit}(G)/X_{CO}^{exit}(G)$ correlation, parameters of the second reaction—z_2 and E_2 are adjusted. Finally, comparing simulated and experimental (or other "reference") dependency of $T_{s,max} = f(p)$, a general order by pressure is applied to all the reactions. Taking into account some minimal influence of each of the reactions on to others, all the parameters should be iterated, thus the total procedure is repeated.

The described procedure in fact provides optimization of a set of the kinetic parameters, although it does not suppose mathematically strict minimization of mean square errors in the seven-dimensional space of parameters. The procedure is performed and discussed below in the article.

Note that the kinetic constants could not be considered universal and applicable for any type of porous media. The *procedure* of the constants generation is more universal in the sense that it allows to adjust the constants to the appropriate "reference" data.

3.4. Method of numerical simulation

The problems (1)–(13) were solved in one-dimensional approximation by using 2DBurner software [42]. This software was designed in Heat and Mass Transfer Institute, Minsk and was used for modeling different FC systems in the past years [35,46].

The homogeneous mesh was used for the problem approximation and solution. The algorithm of solution was optimized for the system of rigid differential equations. After obtaining all the data at the ith time layer, the equation of diffusion together with kinetic equations is discretized by implicit scheme and integrated by Newton's method. On the next step Eqs. (4) and (5) are jointly integrated by the same scheme. For the evaluation of the velocity field Eqs. (1) and (2) are used to generate the Poisson type equation for the pressure at the $i+1$ time layer (modified analog of the MAK method [43]). This equation is solved by the conjugated gradients method or fast Fourier transform [44,45]. The $\Delta x = 1$ mm mesh was used in our simulations. Further decrease of mesh size did not influence simulation results. The time integration step was 10^{-3} s at startup and then gradually grew to 1 s.

Verification of the model was performed in [46] based on the comparison of simulated temperature fields with experimentally measured temperature in the reactor of VOCs oxidation on unsteady startup stage.

4. Results and discussion

The main peculiarity of the experimentally measured correlation $T_{s,max}(G)$ – the very low growth rate at moderate to high flow rates – is not explained adequately in the literature. In the analytical work [18] an explicit formula for porous bed maximum

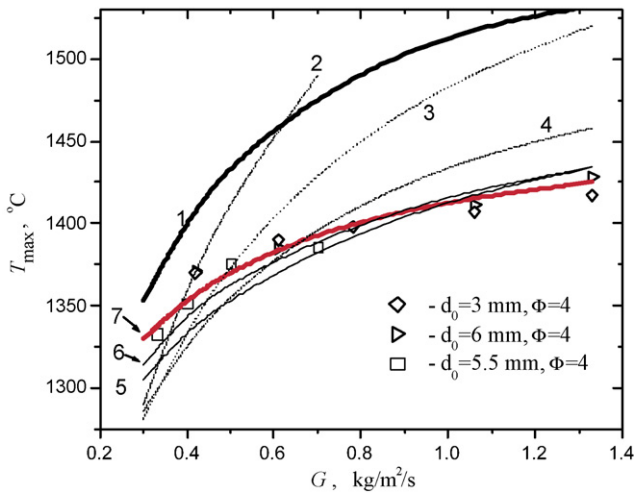

Fig. 4. Porous media maximum temperature. Experimental data [23,24] (marks) and simulation (lines). 1: GRI 3.0 kinetics model; 2: (11)–(13) E_1 = 5000; 3: (11)–(13) E_1 = 15,000; 4: (11)–(13) E_1 = 40,000; 5: (11)–(13) E_1 = 59,000; 6: (11)–(13) E_1 = 79,000; 7: (11)–(13) E_1 = 79,000, λ_s = 0.1. $E_2 = E_3$ = 15,640. Parameters are from Table 2.

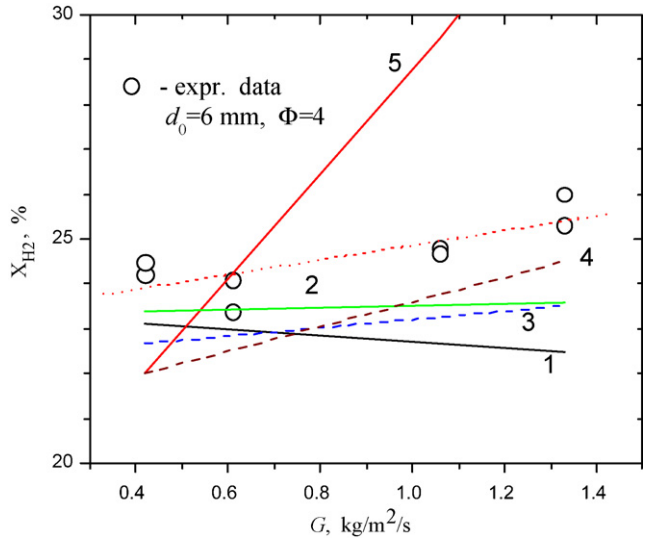

Fig. 5. Hydrogen concentration at the exit of reactor. Experimental data [23,24] (marks) and simulation (lines). 1: E_3 = 25,000 K; 2: E_3 = 40,000 K; 3: E_3 = 59,000 K; 4: E_3 = 79,000 K; 5: E_3 = 99,000 K. $E_1 = E_2$ = 59,000 K. Parameters are from Table 2.

temperature $T_{s,max}$ was obtained:

$$T_{s,max} \approx T_{s,i} = \frac{\Delta T_{ad}}{1 + (\alpha_{vol}\lambda/G^2 c_g^2)} + \frac{E}{\ln(Qz/\alpha_{vol}\Delta T_{ad}(1 + (\alpha_{vol}\lambda/G^2 c_g^2)))}. \quad (15)$$

This equation elucidates that after the first term comes to saturation (high G, low α_{vol} and λ) further temperature growth $T_{s,max}(G)$ acquires logarithmic character. The higher the values of E and z the slower the logarithmic growth is. The direct simulation (see Fig. 4) of the standard case POX reactor demonstrates that the increase of the activation energy E_1 up to 79,000 K (and corresponding increase of pre-exponent z_1) results in $T_{s,max}(G)$ function slowdown which becomes similar enough to the measured correlation. The further increase of activation energy of the main exothermic reaction (11) does not lead to sensitive results. This fact may be explained by the prevailing of the first term in the overall correlation $T_{s,max}(G)$, (15). It is easy to see that contribution of the first term to the total growth rate would be less if values of heat exchange coefficient and thermal conductivity were smaller. (There are certain physical reasons to consider that α_{vol} and λ, as used in conventional FC models, are overestimated: non-steadiness of heat exchange is not considered [25], dispersion includes relaxation component [35]. The discussion of heat and mass transfer sub-models is out of scope of this paper.) In accordance with the above discussion, simulation performed at E_1 = 79,000 K and reduced thermal conductivity (λ_s = 0.1, ε = 0.3) demonstrate smaller steepness of the curve $T_{s,max}(G)$ (Fig. 4). Taking into account limited accuracy of experimental data (~1%) and the fact that very high activation energy slow down calculations E_1 = 59,000 K may be recommended. Note that from chemical kinetics viewpoint the high value of the pre-exponent z may correspond to the chain branching mechanism of the reaction.

The next step is adjusting the parameters of reactions (12) and (13), which determine H_2 and CO concentration at the exit of the reactor. The experimental data demonstrates that H_2 and CO concentration grow with flow rate and maximum temperature (Figs. 2 and 3). Let us calculate correlation $X_{H_2}^{exit}(G)$ for the standard POX reactor while increasing E_3 (Fig. 5). (The z_3 was adjusted simultaneously in order to sustain proper $X_{H_2}^{exit}$ concentration.) The parameters of reactions (11) and (12) are conserved constant, $E_1 = E_2$ = 59,000 K.

The simulation results presented in Fig. 5 show that $X_{H_2}^{exit}(G)$ growth tendency appears at relatively high E_3. The higher E_3 the stronger $X_{H_2}^{exit}(G)$ growth rate is. Actually, not an absolute value of E_3 plays important role, but its relativeness to E_1 value. This fact is explained by the concurrence between reactions (11) and (13) at certain kinetic stage. In general the activation energy of the endothermic reaction (13) should be of the same order or higher than activation energy of exothermic reaction (11) to reproduce $X_{H_2}^{exit}(G)$ growth trend. According to the numerical experiments a reasonable value obtained is E_3 = 59,000 K (Fig. 5).

The next step of the procedure is the kinetic model adjusting by the experimental data of $X_{CO}^{exit}(G)$ or $X_{H_2}^{exit}(G)/X_{CO}^{exit}(G)$. These manipulations are reduced to tuning of the reaction (12) rate constants. The growth rate of $X_{CO}^{exit}(G)$ (in some definite limits) is controlled by activation energy value E_2, and absolute concentration of CO mainly defined by pre-exponential factor z_2. It is important that thermodynamics of the system guarantee simultaneous growth (or decrease) of H_2 and CO concentrations. In this context the tendency of $X_{CO}^{exit}(G)$ growth will be reproduced independently of E_2 value. To approximate the tendency of prevailing growth of CO over H_2 (Fig. 3) rather small value should be attributed to E_2. To demonstrate this peculiarity of the kinetic system the standard POX reactor was simulated at different values of E_2 and fixed parameters of reactions (11) and (13) $E_1 = E_3$ = 59,000 K. Together with E_2 we modified pre-exponent factor z_2 in a way to conserve adequate value of CO concentration $X_{CO}^{exit}(G = 1.3) \approx 12\%$. Results of the numerical simulation together with the basic experimental data [23,24] are presented in Fig. 6. It is easy to see that the tendency of CO prevailing growth can be reproduced at low activation energy E_2 = 5000 K.

Approximation of the experimental correlation $T_{s,max}(p)$ is achieved by assigning the corresponding total pressure order (parameter ORDER) to reactions (11)–(13). As far as no reliable experimental data are available for the pressure-dependent characteristics of POX, we estimated the basic correlation numerically by using detailed GRI 3.0 kinetic mechanism. Taking into account that calculations with the detailed kinetics overestimate the temperature in the system we calculated dimensionless function $T_{s,max}(p)/T_{s,max}(1)$ (where $T_{s,max}(1)$ is the maximum temperature

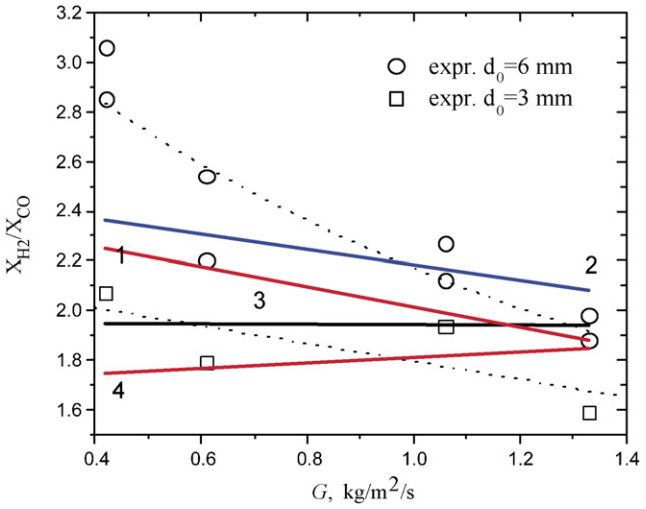

Fig. 6. Experimental data for $X_{H_2}^{exit}(G_m)/X_{CO}^{exit}(G_m)$ [23,24] (marks and approximation—dashed line) and correspondent simulation by model (1)–(13). 1: E_2 = 5000 K; 2: E_2 = 15,000 K; 3: E_2 = 40,000 K; 4: E_2 = 99,000 K. Parameters are from Table 2.

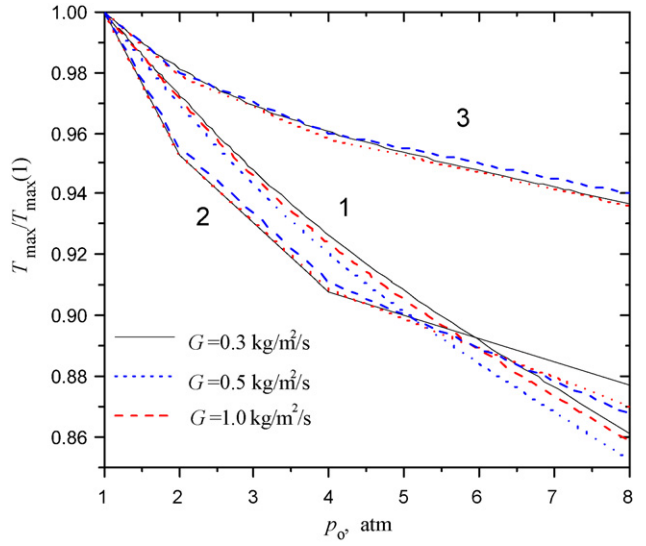

Fig. 7. Dimensionless temperature parameter $T_{max}/T_{max}(1)$ dependence on pressure. 1: numerical evaluation by using GRI 3.0 detailed kinetics; 2: kinetic model (11)–(13), ORDER = 2, 3—kinetic model (11)–(13), ORDER = 1. Reactor parameters of Table 2. Specific mass flow rates are indicated in legend.

in Celsius at p = 1 atm) and used it for ORDER parameter adjusting. This function was calculated with the first and the second order by pressure in (11)–(13) model, while activation energy was fixed: $E_1 = E_3$ = 59,000 K and E_2 = 5000 K. Analyzing the data presented in Fig. 7 one can conclude that the total pressure order of 1.5 may be the optimal for the pressure range from 1 to 4 and given set of other parameters of the model. Obviously better adjusting may be achieved by applying different pressure orders to the reactions (11)–(13).

Because of certain interdependence of the parameters in the set, iteration should be done. By repeating the manipulation one comes soon to a unique set of the model parameters providing good

Table 3
Parameters of the (11)–(13) model elaborated for standard reactor and data of [23,24]

N	Reaction	Parameters
1	$CH_4 + O_2 \xrightarrow{k_1} CO + H_2O + H_2$	z_1 = 16.0e18 m^3/(mol s); E_1 = 59,000 K
2	$2CO + O_2 \overset{k_2, k_{-2}}{\longleftrightarrow} 2CO_2$	z_2 = 5e4 m^3/(mol s); E_2 = 5000 K; z_{-2}, E_{-2} by equilibrium
3	$CH_4 + H_2O \overset{k_3, k_{-3}}{\longleftrightarrow} CO + 3H_2$	z_3 = 2.5e20 m^3/(mol s); E_3 = 59,000 K; z_{-3}, E_{-3} by equilibrium

ORDER = 2.

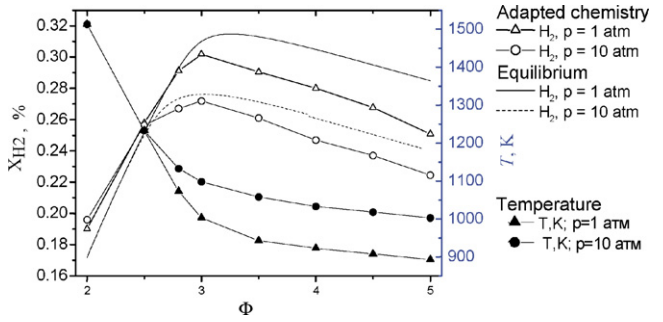

Fig. 8. Comparison of equilibrium H_2 concentration, obtained kinetically by adopted model (11)–(13) and thermodynamically at p = 1 and 10 atm. Methane–air mixture Φ = 2–5. Initial mixture temperature 273 K. Adiabatic process.

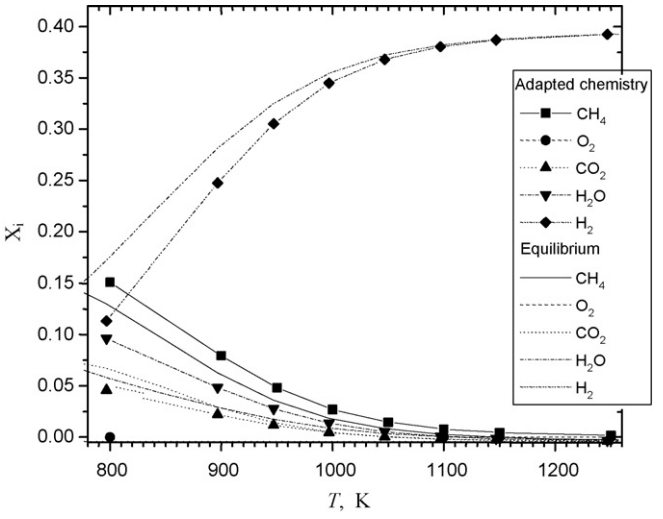

Fig. 9. Comparison of mixture component equilibrium concentrations, obtained kinetically by adopted model (11)–(13) model and thermodynamically at different temperatures. Methane–air mixture Φ = 4, p = 1 atm. Isothermal process.

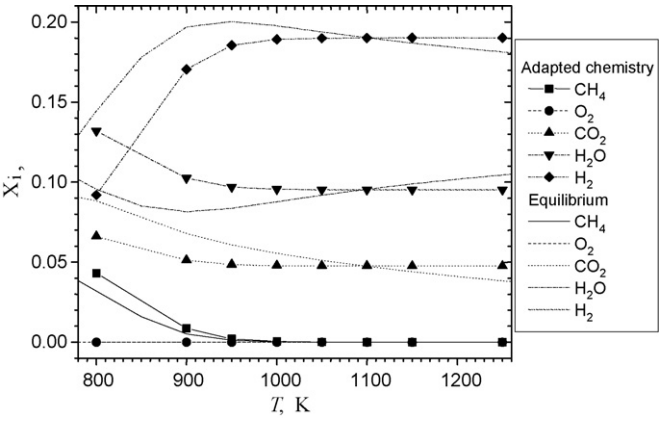

Fig. 10. Comparison of mixture component equilibrium concentrations, obtained kinetically by (11)–(13) model and thermodynamically at different temperatures. Methane–air mixture Φ = 2, p = 10 atm. Isothermal process.

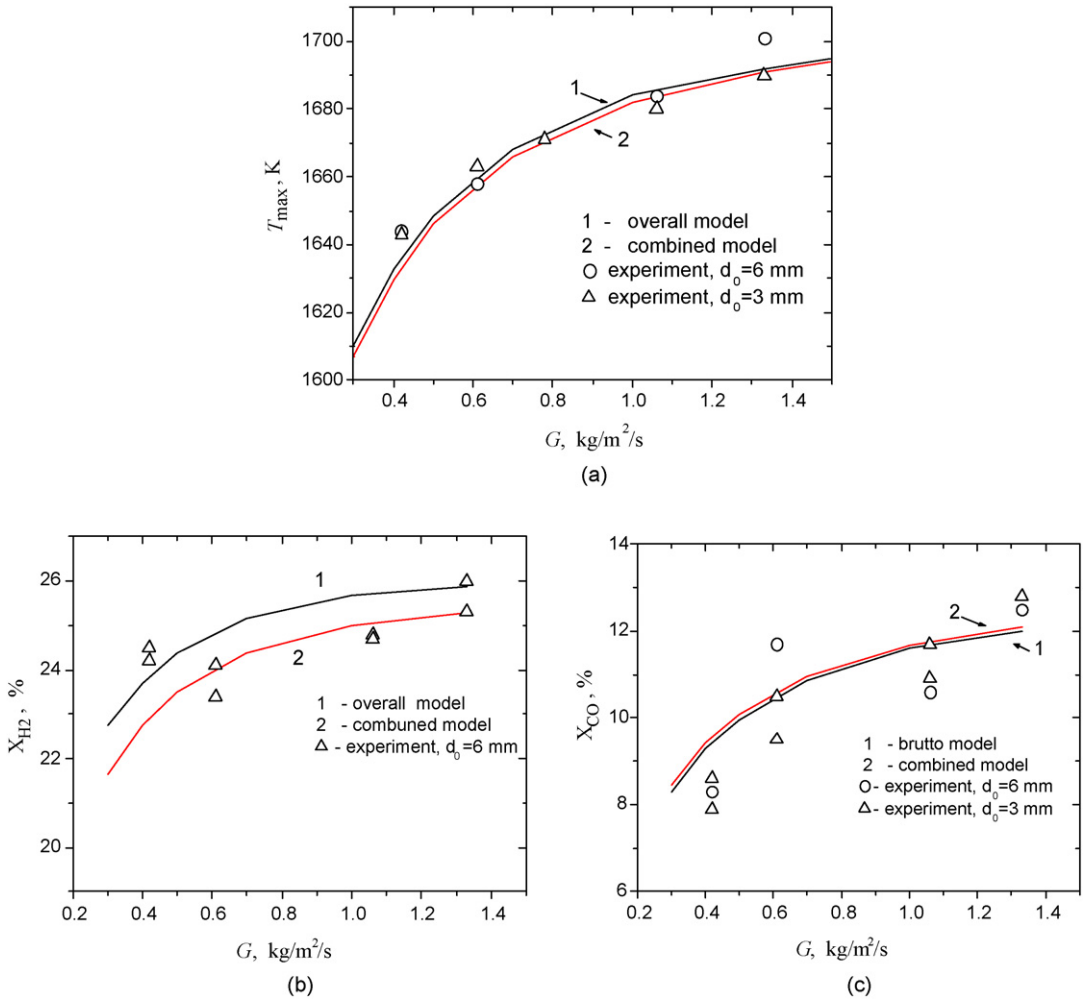

Fig. 11. Maximum temperature of porous medium (a), output concentration of H_2 (b) and CO (c). Calculation by overall model, combined model and experimental data of [23] as depicted in the legend. $\Phi = 4$. Parameters of experiments [23].

(within the general accuracy of the data) reproduction of experimental correlations in a range of operation parameters.

The parameters obtained after iteration are presented in Table 3. It is important to note that obtained chemical model totally correlates with the physical and mathematical model of POX reactor and, to a large extent, compensates the model's mistakes.

The described algorithm of kinetic parameters estimation is not the only possible one. Alternatively to z_3, E_3 estimation by $X_{H_2}^{exit}(G)$ these parameters may be generated via approximation of temperature profile in the endothermic zone of reactor or by other characteristic data. To add, some different experimental data sets may be used for the model tuning. For example, the experimentally measured correlations $T_{s,max}(\Phi)$ and $T_{s,max}(X_{O_2})$ [27,28] may be utilized. Criterion for choosing one or another data set is its correspondence to the practical process, in need of reactor design or optimization.

As far as reverse reaction rates are evaluated via equilibrium constants, the kinetic model guaranties thermodynamic adequacy of the model and reasonable extrapolation capability. The thermodynamic equilibrium calculations made kinetically with the use of the elaborated model are compared with corresponding exact thermodynamic calculations (by EQUILL, CHEMKIN library) (Figs. 8–10). Not perfect correlation in equilibrium concentrations is explained by insufficient freedom degree of the system (11)–(13). Adding equation $CH_4 + CO_2 \leftrightarrow 2CO + 2H_2$ to the system makes equilibrium concentrations and temperatures practically exact. On the other hand, the addition of the new equation demands more complicated adjusting algorithm and bigger experimental data pool.

If the detailed chemical composition of the syngas or influence of the specific additives on the process is of the particular interest the combined model composed of the six-component overall chemical model and detailed gas-phase model (for example GRI 3.0) may be considered. Due to the fact that gas-phase reactions are activated at some higher temperature (compared to the overall model) the basic results obtained for POX system by using both overall and combined models are quite close. The corresponding numerical estimation of the maximum temperature T_{max} and of the output H_2 and CO concentrations are presented in Fig. 11. The temperature and CO concentration estimated by two models coincide with an accuracy of about 1%. The difference between the estimated hydrogen concentrations is somewhat higher (about 4%).

5. Conclusion

The overall three-stage six-component chemical kinetics model is elaborated for extensive numerical study of partial oxidation of methane in inert porous media reactors. The procedure

of the kinetic constants adjustment to experimental data (the temperature–flow rate and the concentration–flow rate correlations) is described. The kinetic constants found for alumina balls packed bed cannot be considered universal and applicable for any type of porous media. The *procedure* of the constants generation is more universal as far as it let one quickly adjust the constants by the appropriate "reference" data.

It is found that extremely slow temperature growth with flow rate $T_{s,max}(G)$, reported for methane (and other hydrocarbons) partial oxidation in inert porous media corresponds to high activation energy of the overall oxidation reactions and may be effectively reproduced by the proposed model. From the viewpoint of the gas-phase chemical kinetics the high values of the pre-exponent factor and activation energy correspond to the chain branching mechanism of the overall reaction.

The mathematical and physical model applied to the system is widely used and proved to be adequate for most filtration combustion problems. Nevertheless transition to the area of parameters where the model is inadequate (for example, inconsistency of radiation diffusion approximation) will automatically question the applicability of the estimated kinetic constants.

If the computation cost is not a critical factor and detailed chemistry of POX process is of a particular interest utilization of the direct sum of the above overall model and detailed chemical kinetics model may be recommended.

References

[1] S. Cornot-Gandolphene, Hydrocarbon feedstock prognosis, Energy Explor. Exploit. 13 (1995) 3.
[2] O. Zhu, X. Zhao, Y. Deng, Advances in the partial oxidation of methane to synthesis gas, J. Nat. Gas Chem. 13 (2004) 191–203.
[3] V.S. Arutiunov, O.V. Krylov, Oxidative Transformations of Methane, Nauka, Moscow, 1998, p. 361.
[4] A.Ya. Rozovski, Dimethylether and gasoline from natural gas, Russ. Chem. J. XLVII (6) (2003) 53–61 (in Russian).
[5] A.P.E. York, T. Xiao, M.L.H. Green, Brief overview of the partial oxidation of methane to synthesis gas, Top. Catal. 22 (3–4) (2003) 345–358.
[6] A.T. Ashcroft, A.K. Cheetham, J.S. Foord, et al., Selective oxidation of methane to synthesis gas using transition metal catalysts, Nature 344 (1990) 319–321.
[7] P.D.F. Vernon, M.L.H. Green, A.K. Cheetham, A.T. Ashcroft, Partial oxidation of methane to synthesis gas, Catal. Lett. 6 (1990) 181–186.
[8] J. Eilers, S.A. Posthuma, S.T. Sie, The shell middle distillate synthesis process (SMDS), Catal. Lett. 7 (1–4) (1990) 253–269.
[9] Gasification Plant Datasheets, 2004 Gasification Database, National Energy Technology Lab., USA, 2004.
[10] F.J. Weinberg, Combustion temperature—the future? Nature 233 (1971) 239–241.
[11] G.A. Fateev, Heat transfer in a reacting porous body during filtration of a gas, Foreign Technology Div. Wright-Patterson AFB Ohio, Accession Number AD0745460, March 10, 1972.
[12] Yu.Sh. Matros, Unsteady Processes in Catalytic Reactors. Studies of Surface Science and Catalysis, Elsevier, 1985, p. 22.
[13] T. Takeno, K. Sato, An excess enthalpy flame theory, Combust. Sci. Technol. 20 (1979) 7–84.
[14] J. Buckmaster, T. Takeno, Blow off and flashback of an excess enthalpy flame: short communication, Combust. Sci. Technol. 25 (1981) 153–158.
[15] V.S. Babkin, Filtration combustion of gases, present state of affairs and prospects, Pure Appl. Chem. 65 (1993) 335–344.
[16] Y. Kotani, H.F. Behbahani, T. Takeno, An excess enthalpy flame combustor for extended flow ranges, in: Proceedings of the 20th (Int.) Symp. on Combustion, vol. 20, 1984, pp. 2025–2033.
[17] J.G. Hoffmann, R. Echigo, H. Yoshida, S. Tada, Experimental study on combustion in a porous media with a reciprocating flow system, Combust. Flame 111 (1997) 32–46.
[18] K.V. Dobrego, S.A. Zhdanok, Engineering calculation of the characteristics of a filtration-combustion wave based on a one-dimensional two-temperature model, J. Eng. Phys. Thermophys. 71 (1) (1998) 420–428.
[19] F.J. Weinberg, T.G. Bartlett, F.B. Carelton, et al., Partial oxidation of fuel-rich mixtures in a spouted bed combustor, Combust. Flame 72 (1988) 235–239.
[20] Y. Itaya, T. Oyashiki, M. Hasastani, Hydrogen production by methane-rich combustion in a ceramic burner, J. Chem. Eng. Jpn. 35 (1) (2002) 46–56.
[21] H. Pedersen-Mjaanes, Hydrogen production from rich combustion inside porous media. MS thesis, University of Cambridge, 2003.
[22] V.V. Gavriliuk, Yu.M. Dmitrenko, S.A. Zhdanok, V.G. Minkina, et al., Methane conversion in a wave of filtration combustion, in: Proceedings of the Fourth International Forum on Heat and Mass Transfer, vol. 4, ITMO Publ., Minsk, 2000, pp. 21–31.
[23] S.A. Zhdanok, Porous media based hydrogen production, in: Proceedings of the Third European Combustion Meeting, Orleans, October 25–28, 2003.
[24] Y.M. Dmitrenko, R.A. Klevan, V.G. Minkina, S.A. Zhdanok, Hydrogen generation by partial oxidation of methane in superadiabatic combustion, in: Proceedings of the Minsk International Colloquium on Physics of Shock Waves, Combustion, Detonation and Non-equilibrium Processes, Minsk, November 12–17, 2005.
[25] S.I. Shabunya, V.V. Martynenko, N.L. Yadrevskaya, A.D. Yakimovich, Modeling of the nonstationary process of conversion of methane to hydrogen in a filtration-combustion wave, J. Eng. Phys. Thermophys. 74 (5) (2001) 1059–1067.
[26] M.K. Drayton, A.V. Saveliev, L.A. Kennedy, A.A. Fridman, Y.E. Li, Superadiabatic partial oxidation of methane in reciprocal and counterflow porous burners, in: Proceedings of the 27th Sympos. (Int.) on Combust., Pittsburg, PA, 1998, pp. 1361–1367.
[27] J.P. Bingue, A.V. Saveliev, A.A. Fridman, L.A. Kennedy, Hydrogen production in ultra-rich filtration combustion of methane and hydrogen sulfide, Int. J. Hydrogen Energy 27 (2002) 643–649.
[28] J.P. Bingue, A.V. Saveliev, L.A. Kennedy, Optimization of hydrogen production by filtration combustion of methane by oxygen enrichment and depletion, Int. J. Hydrogen Energy 29 (2004) 1365–1370.
[29] R. Dhamrat, J. Ellzey, Numerical and experimental study of the conversion of methane to hydrogen in a porous media reactor, Combust. Flame 144 (2006) 698–709.
[30] Z. Al-Hamamre, D. Trimis, K. Wawrzinek, Thermal partial oxidation of methane in porous burners for hydrogen production, in: Proceedings of the Seventh International Conference on Technologies and Combustion for a Clean Environment, Lissabon, Portugal, July, 2003.
[31] L.A. Kennedy, A.A. Fridman, A.V. Saveliev, Superadiabatic combustion in porous media: wave propagation, instabilities, new type of chemical reactor, Int. J. Fluid Mech. Res. 22 (1995) 1–26.
[32] M. Frenclah, H. Wang, M. Goldenberg, G.P. Smith, D.M. Golden, C.T. Bowman, R.K. Hanson, W.C. Gardiner, V. Lissianski, GRI-Mech—an optimized detailed chemical reaction mechanism for methane combustion, Gas Research Institute topical report, GRI-95/0058, 1995.
[33] A.A. Konnov, Detailed reaction mechanism for small hydrocarbons combustion, http://homepages.vub.ac.be/~akonnov/.
[34] J.A. Miller, C.T. Bowman, Mechanism and modeling of nitrogen chemistry in combustion, Prog. Energy Combust. Sci. 15 (1989) 287–338.
[35] K.V. Dobrego, S.A. Zhdanok, Physics of Filtration Combustion of Gases, ITMO Publ., Minsk, 2003, p. 204 (in Russian).
[36] P. Aghalayam, Y.K. Park, F.E. Fernandes, V. Papavasilioyu, A.B. Mhadeshwar, D.G. Vlachos, A C1 mechanism for methane oxidation on platinum, J. Catal. 213 (2003) 23–35.
[37] A.B. Mhadeshwar, D.G. Vlachos, Hierarchical multiscale mechanism development for methane partial oxidation and reforming and for thermal decomposition of oxygenates on Rh, J. Phys. Chem. B 109 (2005) 16819–16835.
[38] N. Wakao, S. Kaguei, Heat and Mass Transfer in Packed Beds, Gordon and Breach Science Publ., New York, 1982, pp. 86–150.
[39] R.J. Kee, F.M. Rupley, J.A. Miller, CHEMKIN-II: A FORTRAN Chemical Kinetics Package for the Analysis of Gas Phase Chemical Kinetics, Sandia National Laboratory, 1989, SAND89-8009B.
[40] F. Contarin, A.V. Saveliev, A.A. Fridman, L.A. Kennedy, A reciprocal flow filtration combustor with embedded heat exchangers: numerical study, Int. J. Heat Mass Transfer 46 (2003) 949–961.
[41] K.V. Dobrego, N.N. Gnezdilov, I.M. Kozlov, V. Bubnovich, H.A. Gonzalez, Numerical investigation of the new regenerator–recuperator scheme of VOC oxidizer, Int. J. Heat Mass Transfer 48 (2005) 4695–4703.
[42] K.V. Dobrego, I.M. Kozlov, N.N. Gnezdilov, V.V. Vasiliev, 2DBurner—Software Package for Gas Filtration Combustion Systems Simulation and Gas Non-steady Flames Simulation. Preprint No. 1, Heat and Mass Transfer Institute Publ., Minsk, 2004.
[43] K.V. Dobrego, I.M. Kozlov, N.N. Gnezdilov, Model and methods of 2D simulation of filtration combustion reactors with arbitrary chemical kinetics, in: Proceedings of the Ninth International Conference on Numerical Combustion, Sorrento, Italy, April 7–10, 2002, pp. 317–318.
[44] R.W. Hockney, J.W. Eastwood, Computer Simulation Using Particles, McGraw-Hill Inc., 1981.
[45] A.J. Harten, High resolution schemes for hyperbolic conservation laws, J. Comput. Phys. 49 (3) (1983) 357–393.
[46] K.V. Dobrego, N.N. Gnezdilov, I.M. Kozlov, E.S. Shmelev, Numerical study and optimization of the porous media VOC oxidizer with electric heating elements, Int. J. Heat Mass Transfer 49 (2006) 5062–5069.
[47] R. Krupiczka, Analysis of thermal conductivity in granular materials, Int. Chem. Eng. 7 (1967) 122–144.